Bioconjugate Chemistry

Communication

pubs.acs.org/bc

Diagnostic Implementation of Fast and Selective Integrin-Mediated Adhesion of Cancer Cells on Functionalized Zeolite L Monolayers

Arianna Greco,[§,†] Laura Maggini,[§,‡,⊥] Luisa De Cola,[*,‡,⊥] Rossella De Marco,[†] and Luca Gentilucci[*,†]

[†]Department of Chemistry "G. Ciamician", University of Bologna, via Selmi 2, 40126 Bologna, Italy

[‡]Institut de science et d'ingénierie supramoléculaires (ISIS), Université de Strasbourg, 8 Allée Gaspard Monge, 67000 Strasbourg, France

[⊥]Institut für Nanotechnologie (INT), Karlsruhe Institute of Technology (KIT) - Campus Nord, Hermann-von-Helmholtz-Platz 1, 76344 Eggenstein-Leopoldshafen, Germany

Supporting Information

ABSTRACT: The rapid and exact identification and quantification of specific biomarkers is a key technology for always achieving more efficient diagnostic methodologies. We present the first application of a nanostructured device constituted of patterned self-assembled monolayers of disk-shaped zeolite L coated with the cyclic integrin ligand c[RGDfK] via isocyanate linker, to the rapid detection of cancer cells. With its high specificity toward HeLa and Glioma cells and fast adhesion ability, this biocompatible monolayer is a promising platform for implementation in diagnostics and personalized therapy formulation devices.

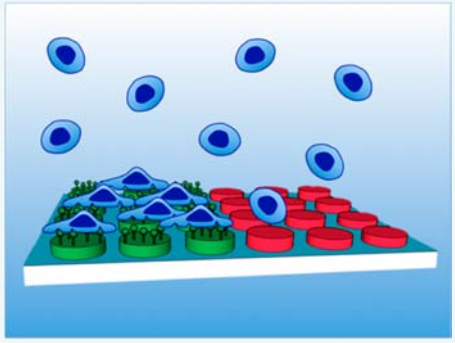

Integrins are heterodimeric glycoproteinic receptors that mediate cellular attachment to the extracellular matrix (ECM) and to other cells.[1−3] Upon interaction with specific ligands (i.e., fibrinogen, fibronectin, plasminogen), they also regulate various cellular functions, such as adhesion, migration, invasion, proliferation, and survival/anoikis.[1,4] There is clear evidence of the crucial role of integrins in a variety of severe diseases, and in particular, the integrins $\alpha v\beta 3$, $\alpha v\beta 5$, $\alpha v\beta 1$, $\alpha 6\beta 4$, and $\alpha 4\beta 1$ are involved in the development of invasive tumors.[4−8]

Since the discovery of the Arg-Gly-Asp (RGD) tripeptide as the minimal recognition motif for many integrins including $\alpha v\beta 3$, $\alpha v\beta 5$, and $\alpha v\beta 1$,[1,9] this sequence has been employed for the design of small-molecule integrin antagonists[4,5,10−14] which led to important results in blocking tumor progression.[15−17] Interest has also recently focused on the construction of RGD-conjugates with anticancer drugs, diagnostic probes, nanoparticles, or nanocarriers, for cancer therapy or imaging.[18−21] Besides, much effort has also been directed to the preparation of RGD-functionalized bioactive surfaces to favor integrin-mediated cell adhesion and growth for biomedical applications, especially implant materials.[22−25] For such uses, long contact times between the substrates and the cells are envisaged. Conversely, much less attention has been paid to the development of RGD-functionalized bioactive surfaces as diagnostic devices to detect cancer cells, for which a fast and yet selective and strong adhesion is preferable. For instance, these devices could be exploited for the entrapment and study of circulating tumor cells (CTCs). CTCs are cells that detach from solid primary tumors during metastasis, entering in the blood circulation. The importance of CTC counting in cancer diagnostics has grown over the past decade,[26−28] as their concentration in the blood represents an indicator of a tumor's invasiveness, allowing monitoring of the therapeutic outcomes of cancer. Moreover, CTCs may serve as a "liquid biopsy" by providing representative tumor tissue, essential for biomarker identification and subsequent formulation of a personalized therapeutic treatment.[29] Current technology platforms for the insulation of CTCs involve immunomagnetic beads or microfluidic devices,[30−33] which both still suffer from low CTC capture.

Based on these premises, herein we present the first implementation of an integrin-targeting nanostructured device constituted of patterned self-assembled monolayers (SAM) of disk-shaped zeolite L[34−38] coated with the cyclic integrin ligand c[RGDfK],[22,39] as a prototype for the rapid and selective detection of cancer cells. The RGD cyclopeptide was specifically chosen for its higher affinity, higher resistance to chemical degradation, and higher selectivity with respect to its linear equivalents.[10] The amino group in the lysine allowed efficient conjugation to the monolayer via isocyanate linker.[18] Zeolite SAMs, previously employed for the construction of cell-growth substrates, were chosen for the large surface area and the possibility of high density of superficial functionalization

Received: June 23, 2015
Revised: August 1, 2015
Published: August 11, 2015

DOI: 10.1021/acs.bioconjchem.5b00350
Bioconjugate Chem. 2015, 26, 1873−1878

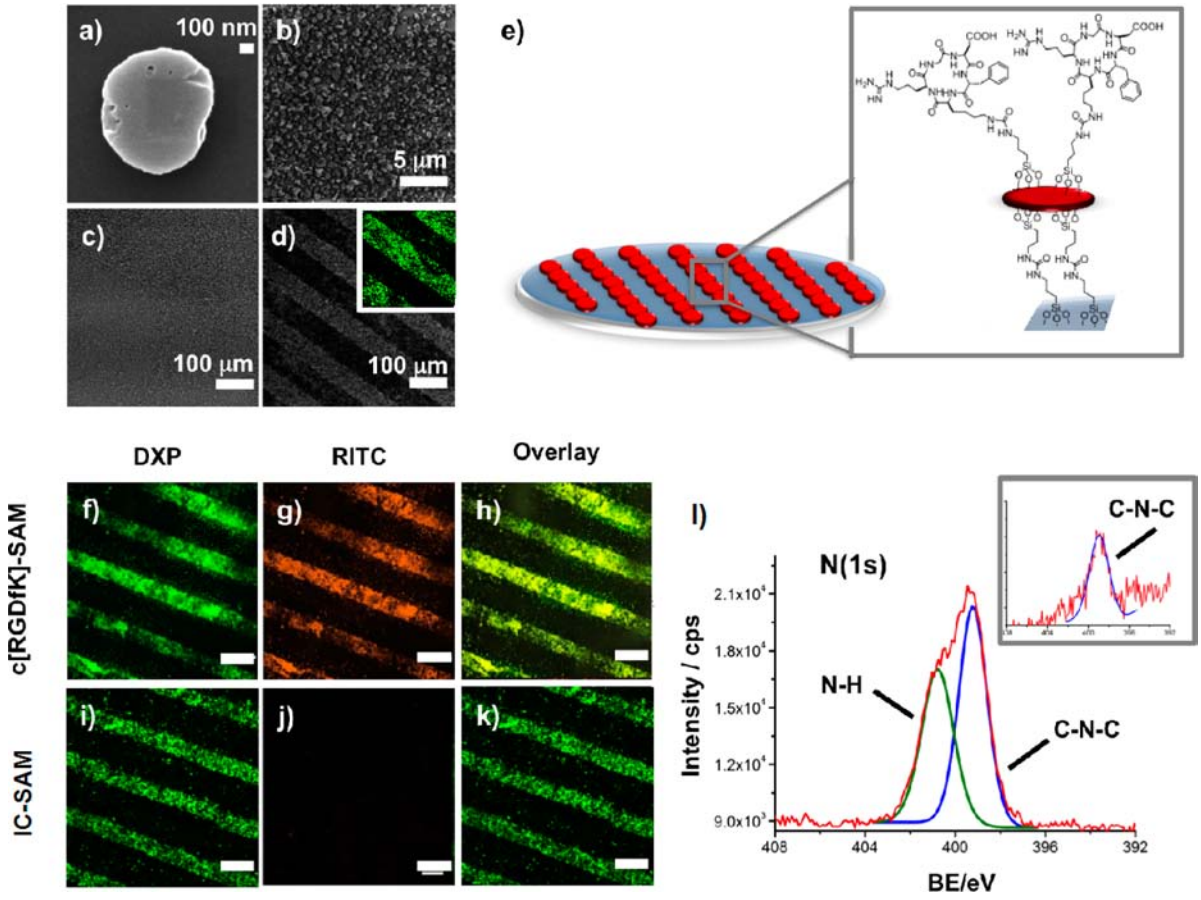

Figure 1. SEM images of (a) zeolite L crystals; (b) DXP-Zeo-IC covalently attached on the surface; SAM before (c) and after (d) PDMS patterning. Inset: confocal image of printed SAM, λ_{exc} = 490 nm. (e) Sketch of the c[RGDfK]-SAM bound onto a glass substrate. (f–h) Confocal images of c[RGDfK]-SAM after reaction with RITC. (i–k) IC-SAM. (f,i) DXP channel (green) λ_{exc}= 490 nm. (g,j) RITC channel (orange) λ_{exc} = 540 nm. (h,k) Overlay. Scale bar = 200 μm. (l) High-resolution N(1s) XPS of c[RGDfK]-SAM. Inset: high-resolution N(1s) XPS of IC-SAM.

with bioactive molecules, providing a large number of contact points, exploitable for a more effective binding to biological systems.[34] The formation of the SAM is achieved by chemical functionalization[34−38,40] of the channel entrances of this porous material, allowing control of the crystal orientation. Furthermore, the organization of the biomolecules on the SAMs can be controlled by microfabrication techniques (i.e., soft lithography and microcontact printing) that allow the creation of predefinite morphologies, dimensions, and molecular orientations.[41−46]

To construct the biocompatible substrate, large and ultraflat disk-shaped zeolite L crystals approximately 1000 nm in width and 250 nm in height (Figure 1a and Supporting Information) were employed.[47] The crystals were first loaded with the fluorescent dye DXP[48] (λ_{exc} = 490 nm; λ_{em} = 564 nm), for visualization purposes (DXP-Zeo), and subsequently their surface was functionalized with ICPTES (DXP-Zeo-IC), for both synthesis of the monolayer and successive grafting of the RGD-cyclopeptide. The characterization of the functionalized zeolites was performed by XPS and TGA. The first technique allowed analysis of the elemental composition of the material upon DXP insertion and subsequent surface functionalization with ICPTES; the very low C(1s) and N(1s) signals for the pristine zeolites, C(1s) 6.1 At%, N(1s) 0.7 At%, increased significantly in DXP-Zeo and DXP-Zeo-IC, C(1s) 20.7 and 33.0 At%, N(1s) 2.0, and 5.5 At%, respectively (Figure S5, Table S1). TGA further confirmed the two functionalization steps by displaying increasing weight loss passing from zeolites; negligible weight loss in the analyzed temperature range, to DXP-Zeo and DXP-Zeo-IC, 1.7% and 5.7% weight loss, respectively, contribution of water excluded, confirming an increasing amount of organic molecules in the hybrids (Figure S6). Ultimately, SEM analysis demonstrated that the morphology of the zeolites was preserved throughout the functionalization steps (Figure S7).

The SAMs were prepared according to a protocol developed in our laboratories (Figure 1).[43,44] Activated silica plates were functionalized with APTES to introduce amino groups on the surface. The coupling with DXP-Zeo-IC, fundamental to the formation of the monolayer, was performed by sonicating the amino-functionalized glass substrates in a suspension of DXP-Zeo-IC in toluene. A stripe-patterned elastomeric PDMS stamp was then pressed onto the DXP-Zeo-IC SAMs (IC-SAMs) and quickly peeled off,[41] leaving stripes of about 50 μm of SAMs on the surface of the glass. This pattern was chosen to better highlight the specific attachment of the cells only on the peptide-functionalized regions of the zeolites.

Once prepared, the printed substrate was coupled with the integrin ligand c[RGDfK]. The cyclopeptide was readily prepared by cyclization of the linear precursor H-Asp(O*t*Bu)-D-Phe-Lys(Boc)-Arg(Mtr)-Gly-OH, obtained in turn by solid-phase peptide synthesis using the acid-labile 2-chlorotrityl resin and the coupling agents TBTU/HOBt/DIPEA under controlled MW heating, according to a recently optimized

DOI: 10.1021/acs.bioconjchem.5b00350
Bioconjugate Chem. 2015, 26, 1873−1878

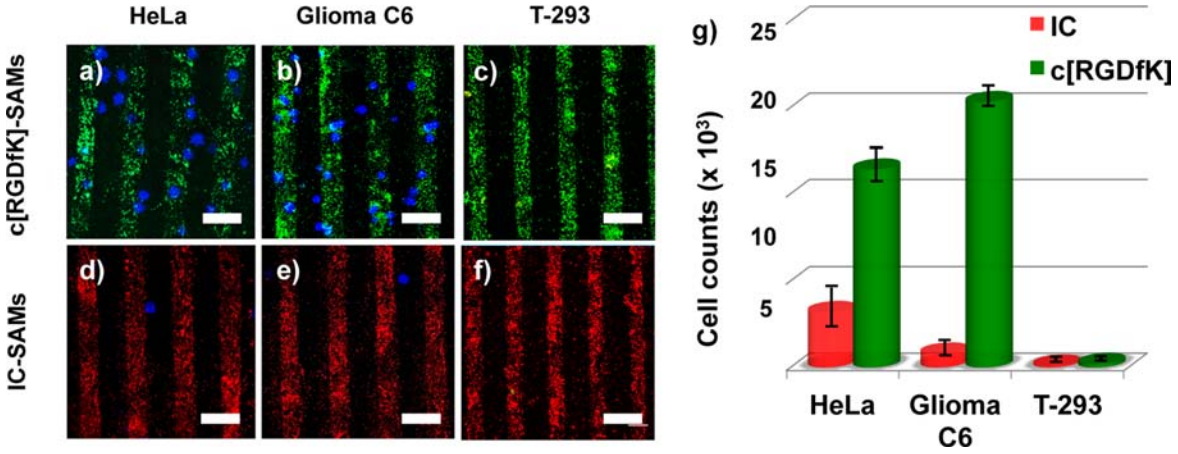

Figure 2. (a–f) Confocal images of c[RGDfK]-SAM (DXP, green channel, λ_{exc}= 490 nm) and IC-SAM (DXP, red channel, λ_{exc} = 490 nm) after 30 min incubation at 37 °C with 1 × 10^5 cancer cells; cells are visualized in blue (DiO staining, λ_{exc} = 484 nm), primary endothelial cells in yellow (DiD, λ_{exc} = 644 nm); scale bar = 100 μm. DXP emission is rendered either in green (a–c) or in red (d–f) for c[RGDfK]-coated or uncoated monolayer, respectively. (g) Number of adhered cells cm^{-2} on c[RGDfK]- and IC-SAMs (analyzed area: 0.0025 cm^2).

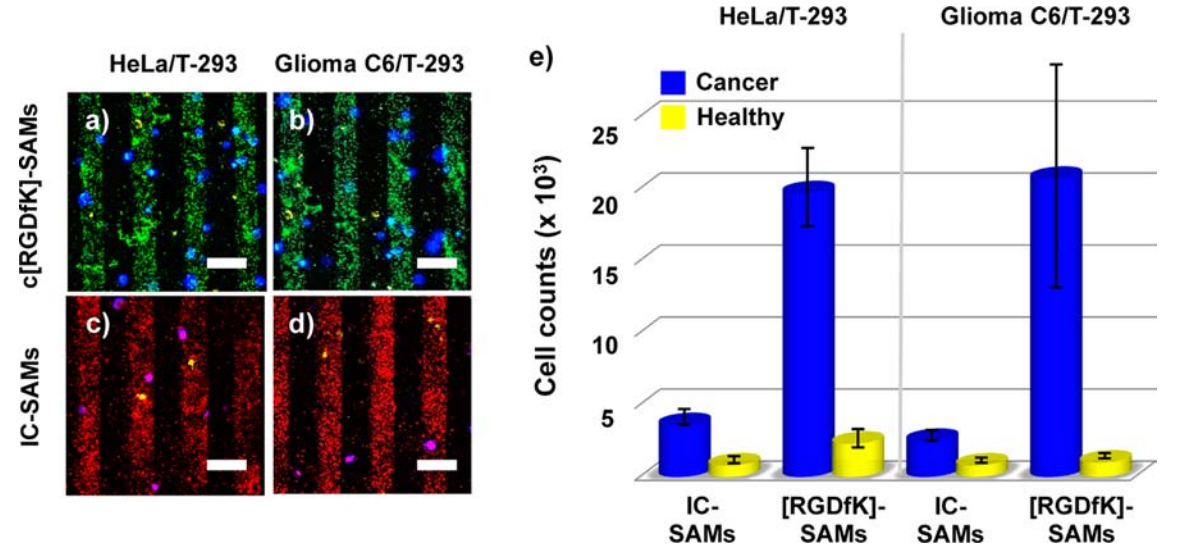

Figure 3. (a–d) Confocal images of c[RGDfK]-functionalized (DXP, green channel, λ_{exc} = 490 nm) and IC-SAMs (DXP, red channel, λ_{exc} = 490 nm) after incubation with a mixed cell population (1 × 10^5 of each cell line, 30 min, 37 °C); cancer cells are visualized in blue (DiO, λ_{exc} = 484 nm), and primary endothelial cells in yellow (DiD, λ_{exc} = 644 nm); scale bar = 100 μm. (e) Number of adhered cells cm^{-2} on c[RGDfK]- and IC-SAMs (analyzed area: 0.0025 cm^2).

procedure.[49] After peptide cleavage with AcOH/TFE, the cyclization was performed by slowly adding the linear peptide to a solution of HATU/DIPEA. The final deprotection with TFA/scavengers afforded the crude cyclopeptide, isolated by semipreparative RP-HPLC. Bioconjugation of the peptide to the printed monolayer was thus ultimately performed upon immersion of the patterned IC-SAMs into a solution of c[RGDfK] and TEA in DMF.

Effective functionalization of the monolayers with the peptide was assessed by XPS analysis and by selective reaction with RITC (Figure 1f–l). Due to its isothiocyanate group, this dye can react with the arginine of c[RGDfK]-SAM, but not with IC-SAM. Accordingly (Figure 1f–h), confocal imaging of the two substrates showed that only c[RGDfK]-SAM presents the characteristic emission of RITC, perfectly superimposable on the signal of the DXP entrapped in the zeolites channels, while the signal of the dye is not present in the IC-SAM (Figure 1i–k), clearly indicating that the presence of the RITC signal in the c[RGDfK]-SAM cannot be due to nonspecific adsorption on the zeolites. Moreover, the images in Figure 1f–h show the exclusive distribution of the dye along the stripes of the surface, highlighting at the same time both the successful patterning and the homogeneous biocoating. XPS analysis of the two substrates further confirmed the increase of C(1s) and N(1s) in the biocoated SAM compared to the nonderivatized monolayer, C(1s) 30.6 and 5.1, N(1s) 42.6 and 8.7 At% for IC-SAM and c[RGDfK]-SAM, respectively. Moreover, the high-resolution XPS of the N(1s) peak for c[RGDfK]-SAM displayed a shape modification compared to IC-SAM (Figure 1l and inset). Indeed, the peak was composed of two signals, at 399 eV (present also in IC-SAM), corresponding to the isocyanate form of N(1s), and at 402 eV, assigned to the peptidic and urea form of N(1s).[50,51]

Once the morphology and the effective surface functionalization of the SAMs were confirmed, adhesion experiments were performed with the integrin expressing cancer cell lines

DOI: 10.1021/acs.bioconjchem.5b00350
Bioconjugate Chem. 2015, 26, 1873–1878

HeLa[52,53] and Glioma C6.[54,55] In order to check the selectivity of the functionalized monolayer toward cancer cells, adhesion experiments were repeated using primary endothelial cells T-293.[56] Primary cells are known to have slower adhesion kinetics[57,58] compared to the cancer cells,[59] and are not expected to be immobilized on a functionalized surface after rapid incubation times.[60] Yet, we determined the adhesion of the primary cells just to be sure that, after the biocoating of our surface, the behavior of these cells would not have changed.[59]

Specifically, 1×10^5 cells of each cell line were stained (DiO staining, λ_{exc} = 484 nm; λ_{em} = 501 nm) and seeded on both IC-SAMs and c[RGDfK]-SAMs, to evaluate any effects of the peptide on the binding activity of the monolayers. After rapid incubation (30 min, 37 °C), cells were washed and fixed with PFA. Confocal microscopy showed that the adhesion behavior on the SAMs of the cancerous cell lines is dramatically different: as shown in Figure 2, the population of both HeLa and Glioma C6 cells on c[RGDfK]-SAMs was much higher than for the nonfunctionalized monolayers.

Accurate counting of the number of cells on the c[RGDfK]-SAMs versus the IC-SAMs showed a 3.5- and 18.4-fold increase of population, for HeLa and Glioma C6, respectively. Increasing incubation times did not lead to significantly higher cell adhesion. Conversely, T-293 cells (DiD staining, λ_{exc}= 644 nm; λ_{em} = 665 nm) did not bind to either c[RGDfK]- or the IC-SAMs. These results demonstrate that cancer cells undergo an efficient integrin-mediated adhesion after a very rapid incubation compared to the lengthy times required for other systems (≥12 h).[41−46]

To further demonstrate that the c[RGDfK]-SAMs could be used for selective detection of cancer cells, we tested cell sensing in the presence of a heterogeneous mixed cell population. Cancer and primary cells (HeLa/T-293 and Glioma C6/T-293 1:1, 1×10^5 each) were stained (cancer cells, DiO, λ_{exc} = 484 nm; λ_{em} = 501 nm; primary cells, DiD, λ_{exc} = 644 nm; λ_{em} = 665 nm) and seeded on both IC-SAMS and c[RGDfK]-SAMs. Confocal microscopy (Figure 3a−d) confirmed very low binding of healthy cells on both substrates.

Most importantly, the number of cancer cells on the peptide-coated SAM was much higher compared to the uncoated SAM, confirming the role of the cyclic peptide in the recognition of the integrin receptors overexpressed on cancer cells. Indeed, the cancer/primary cell ratio increased from 4.5 and 3 for HeLa and Glioma C6, to 8.5 and 20.7, respectively, when passing from the IC-SAMSto the c[RGDfK]-SAMs (Figure 3e).

In conclusion, we have analyzed the selective adhesion of cancer cells to zeolite L SAMs coated with the integrin ligand c[RGDfK] via isocyanate linker. When challenged with a mixed population of cancer and healthy cells, the c[RGDfK]-SAMs showed almost exclusive adhesion of cancer cells. This adhesion was very efficient for HeLa and Glioma C6 cells (up to saturation of the monolayer) upon very rapid incubation, a feature which is expected to favor the implementation to diagnostic device. Modulation of the surface tailoring and its effect on the cell adhesion ability of these monolayers is currently under study. Moreover, exploration of the possibility to investigate the adhered cells by releasing either therapeutic or signaling molecules from the pores of the zeolite SAM is also ongoing. The c[RGDfK]-SAMs conjugate reported herein might represent a potential candidate for the development of new diagnostic kits or even implantable diagnostic devices capable of specifically recognizing and trapping CTCs present in biological fluids, thus enabling a significant advance in the early detection and study of cancer and other integrin-related diseases.

■ ASSOCIATED CONTENT

Supporting Information

The Supporting Information is available free of charge on the ACS Publications website at DOI: 10.1021/acs.bioconjchem.5b00350.

Experimental procedures, materials and methods, including the synthesis of H-Asp(O*t*Bu)-D-Phe-Lys(Boc)-Arg(Mtr)-Gly-OH and of *c*[Arg-Gly-Asp-D-Phe-Lys] (*c*[RGDfK]), spectroscopic characterization data, including ^{1}H NMR (400 MHz, D_2O); preparation of the materials, i.e., zeolites, SAMs, SAMs patterning, SAMs functionalization with the peptide; characterization of the materials and additional figures, including XRD, XPS, TGA, SEM imaging; cell culture, staining, adhesion experiments, and cell counting, and confocal microscopy images for the adhesion experiments of HeLa, Glioma C6, and T-293 cells, onto functionalized and non-functionalized SAMs; references (PDF)

■ AUTHOR INFORMATION

Corresponding Authors

*E-mail: luca.gentilucci@unibo.it. Phone: +39 0512099570. Fax: +39 0512099456.

*E-mail: decola@unistra.fr. Phone: +39 0512099570. Fax: +39 0512099456.

Author Contributions

§L. Maggini and A. Greco contributed equally.

Notes

The authors declare no competing financial interest.

■ ACKNOWLEDGMENTS

For financial support: we thank CHIESI Foundation (Parma, Italy) for the unrestricted support to the project *AsthmaZoè*: Nanostructured materials for the detection of markers of asthma and other correlated inflammatory diseases, 2015-17; MIUR PRIN2010 grant 2008J4YNJY; UniBo (Marco Polo); ERC Advanced Grant, MAGIC 247365; EU MSCA-IEF 627788 "POP-SILICA-"Towards Biodegradable Nanoparticles: Hybrid Organic Mesoporous Silica"; MESR; LDC especially acknowledges AXA Research funds. Laura Caliò, for peptide synthesis; André Devaux, for zeolite synthesis; Pengkun Chen, for XPS analysis; Youssef Atoini, for XRD analysis.

■ ABBREVIATIONS

RGD, Arg-Gly-Asp; SAM, self-assembled monolayer; NP, nanoparticle; DXP, *N,N′*-bis(2,6-dimethylphenyl)perylene-3,4,9,10-tetracarboxylic acid diimide; ICPTES, (3-(isocyano)-propyltriethoxysilane; XPS, X-ray photoelectron spectroscopy; TGA, thermogravimetric analysis; SEM, scanning electron microscopy; APTES, aminopropyltriethoxysilane; PDMS, poly-(dimethylsiloxane); At%, relative atomic percentages; TBTU, *O*-(benzotriazol-1-yl)-*N,N,N′,N′*-tetramethyluronium tetrafluoroborate; HOBt, 1-hydroxybenzotriazole hydrate; DIPEA, *N,N*-diisopropylethylamine; MW, microwave; TFE, CF_3CH_2OH; RITC, rhodamine B isothiocyanate; PFA, paraformaldehyde

DOI: 10.1021/acs.bioconjchem.5b00350
Bioconjugate Chem. 2015, 26, 1873−1878

REFERENCES

(1) Liapis, H., Flath, A., and Kitazawa, S. (1996) Inhibition of skeletal metastasis by ectopic ERα expression in ERα-negative human breast cancer cell lines. *Diagn. Mol. Pathol. 5*, 127−118.

(2) Giancotti, F. G., and Ruoslahti, E. (1999) Integrin signaling. *Science 285*, 1028−1033.

(3) Cooper, C. R., Chay, C. H., and Pienta, K. J. (2002) The role of αvβ3 in prostate cancer progression. *Neoplasia 4*, 191−194.

(4) Sheldrake, H. M., and Patterson, L. H. (2009) Function and antagonism of β3 integrins in the development of cancer therapy. *Curr. Cancer Drug Targets 9*, 519−540.

(5) Hosotani, R., Kawaguchi, M., Masui, T., Koshiba, T., Ida, J., Fujimoto, K., Wada, M., Doi, R., and Imamura, M. (2002) Expression of integrin αvβ3 in pancreatic carcinoma: relation to MMP-2 activation and lymph node metastasis. *Pancreas 25*, e30−35.

(6) Takayama, S., Ishii, S., Ikeda, T., Masamura, S., Doi, M., and Kitajima, M. (2005) The relationship between bone metastasis from human breast cancer and integrin αvβ3 expression. *Anticancer Res. 25*, 79−83.

(7) Desgrosellier, J. S., Cheresh, D. A., and Missan, D. S. (2010) Integrins in cancer: biological implications and therapeutic opportunities. *Nat. Rev. Cancer 10*, 9−22.

(8) Di Persio, M. (2012) Integrin control of tumor invasion. *Crit. Rev. Eukaryotic Gene Expression 22*, 309−324.

(9) Ruoslahti, E., and Pierschbacher, M. D. (1987) New perspectives in cell adhesion: RGD and integrins. *Science 238*, 491−497.

(10) Henry, C., Moitessier, N., and Chapleur, Y. (2002) Vitronectin receptor αvβ3 integrin antagonists: chemical and structural requirements for activity and selectivity. *Mini-Rev. Med. Chem. 2*, 531−542.

(11) Cacciari, B., and Spalluto, G. (2005) Non peptidic αvβ3 antagonists: recent developments. *Curr. Med. Chem. 12*, 51−70.

(12) Urman, S., Gaus, K., Yang, Y., Strijowski, U., Sewald, N., De Pol, S., and Reiser, O. (2007) The constrained amino acid β-Acc confers potency and selectivity to integrin ligands. *Angew. Chem., Int. Ed. 46*, 3976−3978.

(13) Gentilucci, L., Cardillo, G., Spampinato, S., Tolomelli, A., Squassabia, F., De Marco, R., Bedini, A., Baiula, M., Belvisi, L., and Civera, M. (2010) Antiangiogenic effect of dual/selective α5β1/αvβ3 integrin antagonists designed on partially modified retro-inverso cyclotetrapeptide mimetics. *J. Med. Chem. 53*, 106−118.

(14) Cupido, T., Spengler, J., Ruiz-Rodriguez, J., Adan, J., Mitjans, F., Piulats, J., and Albericio, F. (2010) Amide-to-ester substitution allows fine-tuning of the cyclopeptide conformational ensemble. *Angew. Chem., Int. Ed. 49*, 2732−2737.

(15) Hewitt, R. E., Powe, D. G., Morrell, K., Balley, E., Leach, I. H., Ellis, I. O., and Turner, D. R. (1997) Laminin and collagen IV subunit distribution in normal and neoplastic tissues of colorectum and breast. *Br. J. Cancer 75*, 221−229.

(16) Zutter, M. M., Sun, H., and Santoro, S. A. (1998) Altered integrin expression and the malignant phenotype: the contribution of multiple integrated integrin receptors. *J. Mammary Gland Biol. Neoplasia 3*, 191−200.

(17) Rolli, M., Fransvea, E., Pilch, J., Saven, A., and Felding-Habermann, B. (2003) Activated integrin αvβ3 cooperates with metalloproteinase MMP-9 in regulating migration of metastatic breast cancer cells. *Proc. Natl. Acad. Sci. U. S. A. 100*, 9482−9487.

(18) Temming, K., Schiffelers, R. M., Molema, G., and Kok, R. J. (2005) RGD-based strategies for selective delivery of therapeutics and imaging agents to the tumour vasculature. *Drug Resist. Updates 8*, 381−402.

(19) Danhier, F., Le Breton, A., and Préat, V. (2012) RGD-based strategies to target αvβ3 integrin in cancer therapy and diagnosis. *Mol. Pharmaceutics 9*, 2961−2973.

(20) Arosio, D., Casagrande, C., and Manzoni, L. (2012) Integrin-mediated drug delivery in cancer and cardiovascular diseases with peptide-functionalized nanoparticles. *Curr. Med. Chem. 19*, 3128−3151.

(21) Nahrwold, M., Weiβ, C., Bogner, T., Mertink, F., Conradi, J., Sammet, B., Palmisano, R., Royo Gracia, S., Preuβe, T., and Sewald, N. (2013) Conjugates of modified cryptophycins and RGD-peptides enter target cells by endocytosis. *J. Med. Chem. 56*, 1853−1864.

(22) Kantlehner, M., Finsinger, D., Meyer, J., Schaffner, P., Jonczyk, A., Diefenbach, B., Nies, B., and Kessler, H. (1999) Selective RGD-mediated adhesion of osteoblasts at surfaces of implants. *Angew. Chem., Int. Ed. 38*, 560−562.

(23) Kantlehner, M., Schaffner, P., Finsinger, D., Meyer, J., Jonczyk, A., Diefenbach, B., Nies, B., Hölzemann, G., Goodman, S. L., and Kessler, H. (2000) Surface coating with cyclic RGD peptides stimulates osteoblast adhesion and proliferation as well as bone formation. *ChemBioChem 1*, 107−114.

(24) Rechenmacher, F., Neubauer, S., Mas-Moruno, C., Dorfner, P. M., Polleux, J., Guasch, J., Conings, B., Boyen, H. G., Bochen, A., Sobahi, T. R., et al. (2013) A molecular toolkit for the functionalization of titanium-based biomaterials that selectively control integrin-mediated cell adhesion. *Chem. - Eur. J. 19*, 9218−9223.

(25) Mas-Moruno, C., Fraioli, R., Albericio, F., Manero, J. M., and Gil, F. J. (2014) Novel peptide-based platform for the dual presentation of biologically active peptide motifs on biomaterials. *ACS Appl. Mater. Interfaces 6*, 6525−6536.

(26) Gupta, G. P., and Massagué, J. (2006) Cancer metastasis: building a framework. *Cell 127*, 679−695.

(27) Mostert, B., Sleijfer, S., Foekens, J. A., and Gratama, J. W. (2009) Circulating tumor cells (CTCs): detection methods and their clinical relevance in breast cancer. *Cancer Treat. Rev. 35*, 463−474.

(28) Wang, S., Wang, H., Jiao, J., Chen, K.-J., Owens, G. E., Kamei, K.-I., Sun, J., Sherman, D. J., Behrenbruch, C. P., Wu, H., et al. (2009) Three-dimensional nanostructured substrates toward efficient capture of circulating tumor cells. *Angew. Chem., Int. Ed. 48*, 8970−8973.

(29) Punnoose, E. A., Atwal, S. K., Spoerke, J. M., Savage, H., Pandita, A., Yeh, R. F., Pirzkall, A., Fine, B. M., Amler, L. C., Chen, D. S., and Lackner, M. R. (2010) Molecular biomarker analyses using circulating tumor cells. *PLoS One 5*, e12517.

(30) Allard, W. J., Matera, J., Miller, M. C., Repollet, M., Connelly, M. C., Rao, C., Tibbe, A. G., Uhr, J. W., and Terstappen, L. W. (2004) Tumor cells circulate in the peripheral blood of all major carcinomas but not in healthy subjects or patients with nonmalignant diseases. *Clin. Cancer Res. 10*, 6897−6904.

(31) Zieglschmid, V., Hollmann, C., and Böcher, O. (2005) Detection of disseminated tumor cells in peripheral blood. *Crit. Rev. Clin. Lab. Sci. 42*, 155−196.

(32) Nagrath, S., Sequist, L. V., Maheswaran, S., Bell, D. W., Irimia, D., Ulkus, L., Smith, M. R., Kwak, E. L., Digumarthy, S., Muzikansky, A., et al. (2007) Isolation of rare circulating tumour cells in cancer patients by microchip technology. *Nature 450*, 1235−1239.

(33) Adams, A. A., Okagbare, P. I., Feng, J., Hupert, M. L., Patterson, D., Göttert, J., McCarley, R. L., Nikitopoulos, D., Murphy, M. C., and Soper, S. A. (2008) Highly efficient circulating tumor cell isolation from whole blood and label-free enumeration using polymer-based microfluidics with an integrated conductivity sensor. *J. Am. Chem. Soc. 130*, 8633−8641.

(34) Zabala Ruiz, A., Li, H., and Calzaferri, G. (2006) Organizing supramolecular functional dye-zeolite crystals. *Angew. Chem., Int. Ed. 45*, 5282−5287.

(35) Park, J., Bauer, S., von der Mark, K., and Schmuki, P. (2007) Nanosize and vitality: TiO2 nanotube diameter directs cell fate. *Nano Lett. 7*, 1686−1691.

(36) Ferreira, L., Karp, J. M., Nobre, L., and Langer, R. (2008) New opportunities: the use of nanotechnologies to manipulate and track stem cells. *Cell. Stem. Cell. 3*, 136−146.

(37) Böcking, D., Wiltschka, O., Niinimäki, J., Shokry, H., Brenner, R., Lindén, M., and Sahlgren, C. (2014) Mesoporous silica nanoparticle-based substrates for cell directed delivery of Notch signalling modulators to control myoblast differentiation. *Nanoscale 6*, 1490−1498.

(38) Kehr, N. S., Galla, H.-J., Riehemann, K., and Fuchs, H. (2015) Self-assembled monolayers of enantiomerically functionalized periodic mesoporous organosilicas and the effect of surface chirality on cell adhesion behaviour. *RSC Adv. 5*, 5704−5710.

DOI: 10.1021/acs.bioconjchem.5b00350
Bioconjugate Chem. 2015, 26, 1873−1878

(39) Haubner, R., Finsinger, D., and Kessler, H. (1997) Stereoisomeric peptide libraries and peptidomimetics for designing selective inhibitors of the αvβ3 integrin for a new cancer therapy. *Angew. Chem., Int. Ed. Engl. 36*, 1374−1389.
(40) Yoon, K. B. (2007) Organization of zeolite microcrystals for production of functional materials. *Acc. Chem. Res. 40*, 29−40.
(41) Xia, Y., and Whitesides, G. M. (1998) Soft lithography. *Angew. Chem., Int. Ed. 37*, 550−575.
(42) Alves, N. M., Pashkuleva, I., Reis, R. L., and Mano, J. F. (2010) Controlling cell behavior through the design of polymer surfaces. *Small 6*, 2208−2220.
(43) Kehr, N. S., Schaefer, A., Ravoo, B. J., and De Cola, L. (2010) Asymmetric printing of molecules and zeolites on self assembled monolayers. *Nanoscale 2*, 601−605.
(44) Kehr, N. S., Riehemann, K., El-Gindi, J., Schäfer, A., Fuchs, H., Galla, H.-J., and De Cola, L. (2010) Cell adhesion and cellular patterning on a self-assembled monolayer of zeolite L crystals. *Adv. Funct. Mater. 20*, 2248−2254.
(45) Sakakibara, K., Hill, J. P., and Ariga, K. (2011) Thin-film-based nanoarchitectures for soft matter: controlled assemblies into two-dimensional worlds. *Small 7*, 1288−1308.
(46) El-Gindi, J., Benson, K., De Cola, L., Galla, H. J., and Seda Kehr, N. (2012) Cell adhesion behavior on enantiomerically functionalized zeolite L monolayers. *Angew. Chem., Int. Ed. 51*, 3716.
(47) Devaux, A., Calzaferri, G., Miletto, I., Cao, P., Belser, P., Brühwiler, D., Khorev, O., Häner, R., and Kunzmann, A. (2013) Self-absorption and luminescence quantum yields of dye-zeolite L composites. *J. Phys. Chem. C 117*, 23034−23047.
(48) Busby, M., Devaux, A., Blum, C., Subramaniam, V., Calzaferri, G., and De Cola, L. (2011) Interactions of perylene bisimide in the one dimensional channels of zeolite L. *J. Phys. Chem. C 115*, 5974−5988.
(49) Yamada, K., Nagashima, I., Hachisu, M., Matsuo, I., and Shimizu, H. (2012) Efficient solid-phase synthesis of cyclic RGD peptides under controlled microwave heating. *Tetrahedron Lett. 53*, 1066−1070.
(50) Liu, S., Tian, J., Wang, L., Zhang, Y., Qin, X., Luo, Y., Asiri, A. M., Al-Youbi, A. O., and Sun, X. (2012) Hydrothermal treatment of grass: a low-cost, green route to nitrogen-doped, carbon-rich, photoluminescent polymer nanodots as an effective fluorescent sensing platform for label-free detection of Cu(II) ions. *Adv. Mater. 24*, 2037−2041.
(51) Yang, Z., Xu, M., Liu, Y., He, F., Gao, F., Su, Y., Wei, H., and Zhang, Y. (2014) Nitrogen-doped, carbon-rich, highly photoluminescent carbon dots from ammonium citrate. *Nanoscale 6*, 1890−1895.
(52) Chattopadhyay, N., and Chatterjee, A. (2001) Role of αvβ3 integrin receptor in the invasive potential of human cervical cancer (SiHa) cells. *J. Environ. Pathol., Toxicol. Oncol. 20*, 11−21.
(53) Choi, D. S., Jin, H. E., Yoo, S. Y., and Lee, S. W. (2014) Cyclic RGD peptide incorporation on phage major coat proteins for improved internalization by HeLa cells. *Bioconjugate Chem. 25*, 216−223.
(54) Malek-Hedayat, S., and Rome, L. H. (1992) Expression of multiple integrins and extracellular matrix components by C6 glioma cells. *J. Neurosci. Res. 31*, 470−478.
(55) Mattern, R. H., Read, S. B., Pierschbacher, M. D., Sze, C. I., Eliceiri, B. P., and Kruse, C. A. (2005) Glioma cell integrin expression and their interactions with integrin antagonists. *Cancer Ther. 3A*, 325−340.
(56) Taherian, A., Li, X., Liu, Y., and Haas, T. A. (2011) Differences in integrin expression and signaling within human breast cancer cells. *BMC Cancer 11*, 293.
(57) Roberts, C., Chen, C. S., Mrksich, M., Martichonok, V., Ingber, D. E., and Whitesides, G. M. (1998) Using mixed self-assembled monolayers presenting RGD and (EG)3OH groups to characterize long-term attachment of bovine capillary endothelial cells to surfaces. *J. Am. Chem. Soc. 120*, 6548−6555.
(58) Reinhart-King, C. A., Dembo, M., and Hammer, D. A. (2005) The dynamics and mechanics of endothelial cell spreading. *Biophys. J. 89*, 676−689.
(59) Orgovan, N., Peter, B., Bösze, S., Ramsden, J. J., Szabó, B., and Horvath, R. (2014) Dependence of cancer cell adhesion kinetics on integrin ligand surface density measured by a high-throughput label-free resonant waveguide grating biosensor. *Sci. Rep. 4*, 4034.
(60) Reinhart-King, C. A., Hammer, D. A., Mott, R. E., Helmke, B. P., Boettiger, D., Stamenović, D., Wang, N., Ingber, D. E., Lomakina, E., Waugh, R. E. et al. (2006) *Principles of Cellular Engineering: Understanding the Biomolecular Interface Hardcover* (King, M. R., Ed.) Academic Press, Burlington, MA.

DOI: 10.1021/acs.bioconjchem.5b00350
Bioconjugate Chem. 2015, 26, 1873−1878